NANO LETTERS

Letter

pubs.acs.org/NanoLett

Polymer Nanofibers Embedded with Aligned Gold Nanorods: A New Platform for Plasmonic Studies and Optical Sensing

Pan Wang,[†] Lei Zhang,[†,‡] Younan Xia,[‡] Limin Tong,*[,†] Xia Xu,[§] and Yibin Ying[§]

[†]State Key Laboratory of Modern Optical Instrumentation, Department of Optical Engineering, Zhejiang University, Hangzhou, Zhejiang 310027, China

[‡]The Wallace H. Coulter Department of Biomedical Engineering, Georgia Institute of Technology and Emory University, Atlanta, Georgia 30332, United States

[§]College of Biosystems Engineering and Food Science, Zhejiang University, Hangzhou, Zhejiang 310027, China

Supporting Information

ABSTRACT: This paper reports the fabrication and characterization of polymer nanofibers embedded with gold nanorods in uniaxial alignment for applications in optical waveguiding and sensing. Using a waveguiding approach, we demonstrated highly efficient excitation of localized surface plasmon resonance in the embedded gold nanorods with a photon-to-plasmon-conversion efficiency as high as 70% for a single nanorod at its longitudinal resonance wavelength. On the basis of waveguiding polymer nanofibers embedded with gold nanorods, we further demonstrated compact optical humidity sensors with a response time of 110 ms and an operation optical power as low as 500 pW.

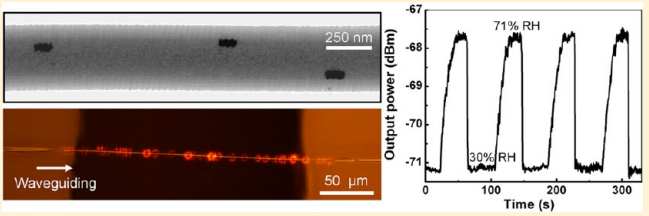

KEYWORDS: *Gold nanorods, polymer nanofibers, waveguides, surface plasmon resonance, optical sensing*

Owing to their shape- and size-dependent optical properties known as localized surface plasmon resonance (LSPR), noble-metal nanoparticles are finding use in a range of emerging applications such as biological and chemical sensing,[1−3] surface-enhanced Raman spectroscopy,[4−6] biomedicine,[7−10] and nanophotonics.[11−13] For the fabrication of devices, one essential step is to incorporate the nanoparticles in a solid matrix (e.g., polymer or glass) to generate complex one- or multidimensional building blocks. In addition to the widely exploited forms such as thin films or bulk materials,[14−19] the incorporation of nanoparticles in nanofibers or nanowires[20−24] has recently received intensive attention due to the high flexibility and versatility in the construction of nanoelectronic or nanophotonic devices and circuits with one-dimensional nanostructures.[25−27] To date, LSPR excitation in nanoparticles is commonly realized using free-space irradiation.[17−19,21−24] Because of the small extinction cross section of a single nanoparticle and the relatively large irradiation area of a free-space light beam, the efficiency of photon-to-plasmon conversion is rather limited. In addition, to redirect a light beam to a nanoparticle in free space, bulky components (e.g., prisms or objectives) are often required, making it difficult to realize nanoparticle-based photonic devices with miniaturized sizes and low operation optical powers. With the use of waveguiding polymer nanofibers embedded with gold nanorods (GNRs), here we demonstrated a highly efficient approach to photon-to-plasmon conversion in GNRs with high compactness. The nanofibers were directly drawn from a polymer solution containing GNRs, which were uniaxially aligned along the long axes of the fibers. When light was coupled into and guided through a single nanofiber, LSPR in the embedded GNRs could be efficiently excited with strong collective polarization dependence. Using a nanofiber of 350 nm in diameter and embedded with a single GNR of 101 nm × 37 nm, we further demonstrated a photon-to-plasmon-conversion efficiency up to 70% at its longitudinal resonance wavelength. Finally, based on waveguiding nanofibers embedded with GNRs, we also demonstrated optical humidity sensors with small footprints, fast response, ultralow optical power consumption, and high photochemical stability.

GNRs were synthesized using a seed-mediated method[28] described in detail in the Supporting Information. The as-prepared GNRs had an aspect ratio of ∼2.5 (Figure S1 in Supporting Information) and their aqueous suspension showed ensemble transverse (T-SPR) and longitudinal surface plasmon resonance (L-SPR) peaks at 517 and 696 nm (Figure S2 in Supporting Information), respectively. Polyacrylamide (PAM), a hydrophilic polymer, was used to host the GNRs and for drawing nanofibers. To prevent the GNRs from aggregation in a PAM solution, we coated their surface with a layer of poly(sodium 4-styrenesulfonate) (see Supporting Information including Figure S3 for details).[29]

To produce GNR-embedded nanofibers, we used a direct solution drawing technique (see Supporting Information including Figure S4 for details), which shares the principle of

Received: March 18, 2012
Revised: May 8, 2012
Published: May 14, 2012

electrospinning,[27] but is capable of generating nanofibers with higher optical quality in terms of optical waveguiding loss (typically lower than 0.1 dB/mm for pure nanofibers).[30−32] Figure 1a shows scanning electron microscopy (SEM) images

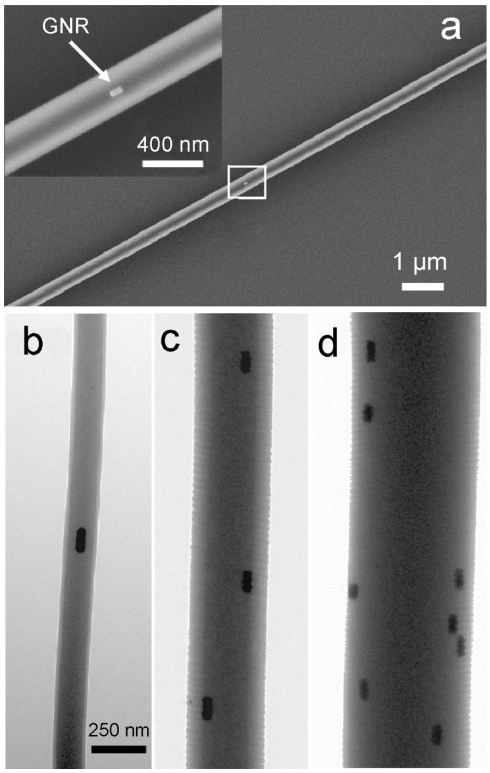

Figure 1. (a) SEM image of a GNRs/PAM nanofiber of 340 nm in diameter. The inset shows a close-up image of the nanofiber where a GNR was positioned close to the surface. (b−d) TEM images of GNRs/PAM nanofibers with diameters of 150, 360, and 600 nm, respectively. The scale bar in (b) is applicable to both (c,d).

of a PAM nanofiber that contained many GNRs. The nanofiber had a uniform diameter of ∼340 nm, together with a smooth surface. One of the GNRs positioned close to the surface of the nanofiber could be clearly seen (also see the inset). For better resolution, we used transmission electron microscopy (TEM) to investigate individual GNRs embedded in PAM nanofibers. Figure 1b−d shows TEM images of GNRs/PAM nanofibers with diameters of 150, 360, and 600 nm, respectively. The GNRs were more or less aligned parallel to the long axes of the nanofibers, together with a density around 13 μm^{-3}. To investigate the orientation distribution of the GNRs, we analyzed 150 GNRs within a nanofiber of 110 μm in length (the same one shown in Figure 1c) by TEM imaging. We found that over 90% of the GNRs were aligned parallel (within ±3°) to the long axis of the nanofiber (Figure S5 in Supporting Information). The unidirectional alignment of GNRs in PAM nanofibers can be attributed to the strong shear forces exerted on the nanorods during a fiber drawing process.[24,33]

To investigate optical properties of individual GNRs/PAM nanofibers, we used a beam of unpolarized white light (SC450, Fianium Ltd.) from a standard optical fiber to illuminate a nanofiber at an oblique angle of about 30° with respect to the nanofiber's long axis. We used a 20× objective (NA = 0.4, CFI LU Plan BD ELWD, Nikon) to collect the scattered light, which was then redirected to a spectrometer (iHR 550, Horiba Jobin Yvon) and a charge-coupled device (CCD) camera (DS-Fi1c, Nikon) after passing through a linear polarizer for polarization selection (Figure 2a). Figure 2b,c shows dark-field images of a GNRs/PAM nanofiber of 440 nm in diameter and 4.1 mm in length that were taken at parallel and perpendicular polarizations, respectively. At parallel polarization, the scattered light showed a bright red color (Figure 2b), while at perpendicular polarization, the scattered light gave a weak green color (Figure 2c). The strong polarization-dependent scattering along the whole nanofiber, which resembles the anisotropic optical response of individual GNRs (Figure S6 in Supporting Information), intuitively verifies the long-range unidirectional alignment of GNRs in the nanofiber. Figure 2d shows scattering spectra of the nanofiber obtained at different polarization angles, clearly showing the suppression of T-SPR (L-SPR) band at parallel (perpendicular) polarization. Compared to those dispersed in water (Figure S2b in Supporting Information), the GNRs in PAM nanofibers showed an obvious red shift from 696 to 750 nm for the L-SPR peak (Figure 2d, also see Figure S7 in Supporting Information for spectrum taken without polarization selection), which can be attributed to an increase in refractive index (1.54 vs 1.33 for PAM and water).[34] In addition, by reducing the concentration of GNRs in the PAM solution, PAM nanofibers with GNRs at extremely low densities could be fabricated. Figure 2e,f shows typical dark-field images of nanofibers with the densities of GNRs around 0.8 and 0.2 μm^{-3}, respectively. Although these sparsely distributed GNRs were difficult to identify by TEM imaging, they could be readily visualized from the dark-field images.

Benefited from the favorable optical waveguiding properties of the solution-drawn polymer nanofibers,[31,32] the LSPR of the embedded GNRs could be excited by a waveguiding approach, as schematically illustrated in Figure 3a. Briefly, guided light in a standard optical fiber was squeezed into a fiber taper drawn from the same fiber[35] and then evanescently coupled into guiding modes of a GNRs/PAM nanofiber suspended across a microchannel.

Experimentally, we used a white light from a halogen lamp as a broadband source. To estimate the coupling efficiency between the fiber taper and the nanofiber, we launched light from one side of a pure PAM nanofiber suspended across a MgF_2 microchannel of 390 μm in width, measured output at the other side (Figure 3b), and obtained a coupling efficiency of ∼80%. Using the same scheme, we studied a GNRs/PAM nanofiber of 590 nm in diameter suspended across the same microchannel. With an optical power as low as 50 nW (measured at the output end of the fiber taper used for launching), light scattered from the embedded GNRs was observed along the nanofiber (Figure 3c). For comparison, white light with the same power guided in pure PAM nanofibers did not exhibit observable scattering (Figure 3b). Similar to the illumination scheme, strong polarization-dependent light scattering was observed along the waveguiding nanofiber (Figure 3d,e). Since the embedded GNRs were aligned parallel to the fiber's long axis and usually a large fraction of the guiding modes of a wavelength-scale nanofiber was in perpendicular polarization,[36] the T-SPR band of the GNRs was excited more efficiently than the L-SPR band, resulting in faster damping of T-SPR band in cascaded GNRs along the length of the nanofiber. As shown in Figure 3c, the color of the scattered light changed from yellowish-green in the left portion to red in the right portion of the nanofiber with

dx.doi.org/10.1021/nl301055f | Nano Lett. 2012, 12, 3145−3150

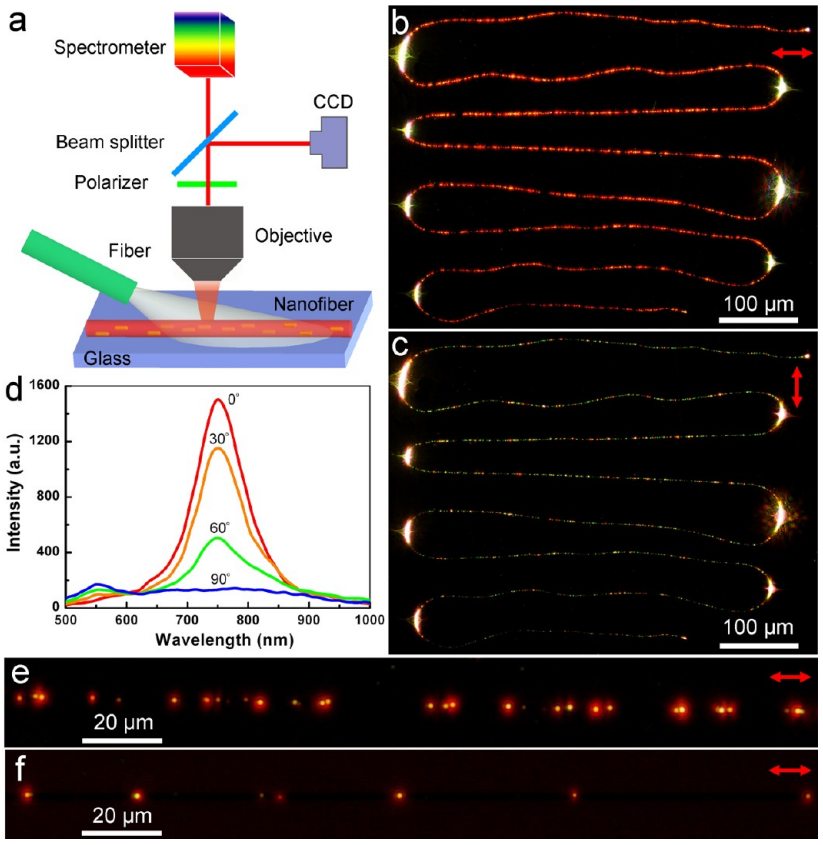

Figure 2. (a) Schematic illustration of dark-field setup for light scattering imaging and spectroscopy. (b,c) Dark-field images of a GNRs/PAM nanofiber of 440 nm in diameter and 4.1 mm in length taken at parallel and perpendicular polarizations, respectively. The bright white spots at the turnings correspond to the light scattered by the nanofiber. (d) Scattering spectra of the nanofiber obtained at different polarization angles. (e,f) Dark-field images (taken at parallel polarization) of nanofibers with the densities of GNRs around 0.8 and 0.2 μm^{-3}, respectively.

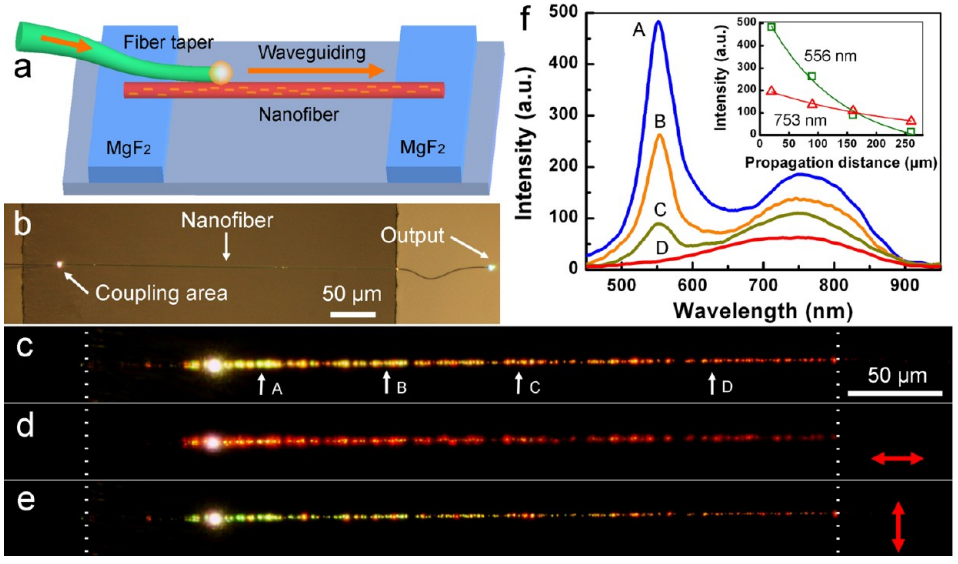

Figure 3. (a) Schematic illustration of waveguiding excitation of a microchannel-supported GNRs/PAM nanofiber using a fiber taper. (b) Optical microscopy image of coupling a white light into a pure PAM nanofiber of 470 nm in diameter. (c–e) Optical microscopy images of waveguiding excitation of GNRs embedded in a PAM nanofiber of 590 nm in diameter. The images in (d,e) were taken at polarization parallel and perpendicular to the nanofiber, respectively. The scale bar in (c) is applicable to both (d,e). White dotted lines are drawn to help identify the boundary of the microchannel. (f) Spatially resolved scattering spectra collected at four positions indicated by white arrows in (c). Inset, intensity of the scattered light at two LSPR peaks (556 and 753 nm) as a function of propagation distance. The intensity was fitted using a first-order exponential function.

decreasing intensity. For reference, spatially resolved scattering spectra (Figure 3f) collected at four positions along the long axis of the nanofiber (Figure 3c) clearly show the evolution of spectral components from yellowish-green at position A to red at position D. The inset of Figure 3f shows the intensity of scattered light as a function of the propagation distance for

dx.doi.org/10.1021/nl301055f | *Nano Lett.* 2012, 12, 3145–3150

both LSPR peaks, which exhibited an exponential decay along the length of the nanofiber, with measured extinction coefficients of 79 cm^{-1} (waveguiding loss ~34 dB/mm) at 556 nm and 41 cm^{-1} (waveguiding loss ~18 dB/mm) at 753 nm, respectively. In comparison, at a wavelength (e.g., 980 nm) away from LSPR bands of the GNRs, the nanofibers showed a greatly reduced waveguiding loss of ~7 dB/mm (Figure S8 in Supporting Information).

It is worth noting that the peak extinction cross section of a single GNR, typically ranging from 10^3 to 10^4 nm^2,[28] is comparable to the mode area of a nanofiber (about 10^4 to 10^5 nm^2, depending on the cross section of the nanofiber[37]). When the light is guided through the nanofiber, the guiding modes maintain their small mode areas all the way along the entire length of the nanofiber, enabling strong interaction between the light and the embedded GNRs in cascade and making it possible to transfer light to LSPR in GNRs with high efficiency. For reference, from the optical microscopy images obtained under waveguiding excitation and light illumination (Figure S9 in Supporting Information), we determined that for a 100 μm long section of GNRs/PAM nanofiber with a diameter of 590 nm waveguiding excitation offered an excitation efficiency of nearly 100- (for the T-SPR band) or 35-fold (for the L-SPR band) higher than the illumination scheme (see Supporting Information for details).

Using waveguiding excitation, it was also possible to investigate the LSPR of a single GNR in a nanofiber. As shown in Figure 4a, when a 35 nW white light was launched into a nanofiber of 350 nm in diameter, which only contained one GNR (Figure 4b, the dimensions of the GNR were 101 nm × 37 nm), a single bright scattering spot was observed. The scattering spectrum of the GNR is given in Figure 4c, clearly showing both T-SPR (552 nm) and L-SPR (783 nm) peaks. It is worth noting that unlike the spectra shown in Figure 3f the L-SPR peak dominated the spectrum, which can be explained as a result of the increase in longitudinal electric field component for the nanofiber with a deep-subwavelength size. To estimate the photon-to-plasmon-conversion efficiency of a single GNR in a waveguiding nanofiber, we used an evanescent coupling technique to measure and compare the power of waveguiding light before and after the GNR (Figure S10 in Supporting Information). For guided light with a wavelength of 532 nm close to the T-SPR peak (Figure 4d), the measured photon-to-plasmon-conversion efficiency of the GNR was ~20%. For guided light with a wavelength of 785 nm that coincided with the L-SPR peak (Figure 4e), the conversion efficiency went up to 70%.

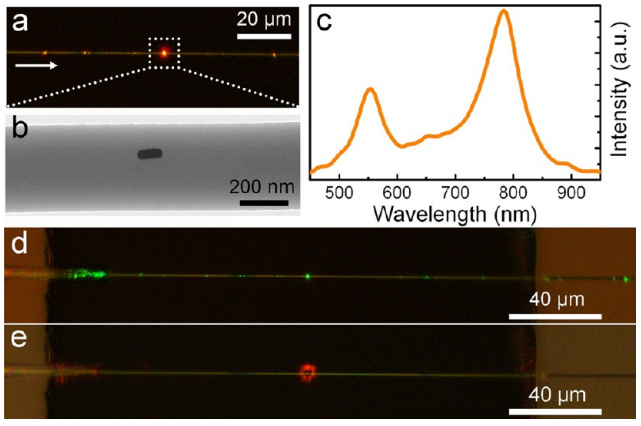

Figure 4. (a) Optical microscopy image of a single GNR embedded in a waveguiding nanofiber of 350 nm in diameter and excited by a white light. White arrow indicates the direction of light propagation. (b) TEM image of the embedded GNR in (a). (c) Scattering spectrum of the waveguiding excited GNR shown in (a). (d,e) Optical microscopy images of the nanofiber waveguiding monochromatic lasers with wavelengths of 532 and 785 nm, respectively.

The highly efficient photon-to-plasmon conversion of single GNRs in waveguiding nanofibers may greatly facilitate and enhance light-matter interactions within a highly localized area[38] and open up opportunities for developing GNR-based photonic components and devices with miniaturized sizes, high compactness, and low optical power consumption. To demonstrate this capability, we also applied the GNRs/PAM nanofibers to optical relative humidity (RH) sensing.

We first investigated the spectral shift of LSPR of a single embedded GNR when exposed to different levels of humidity. As shown in Figure 5a, we suspended a PAM nanofiber of 330 nm in diameter containing a single GNR (100 nm × 40 nm)

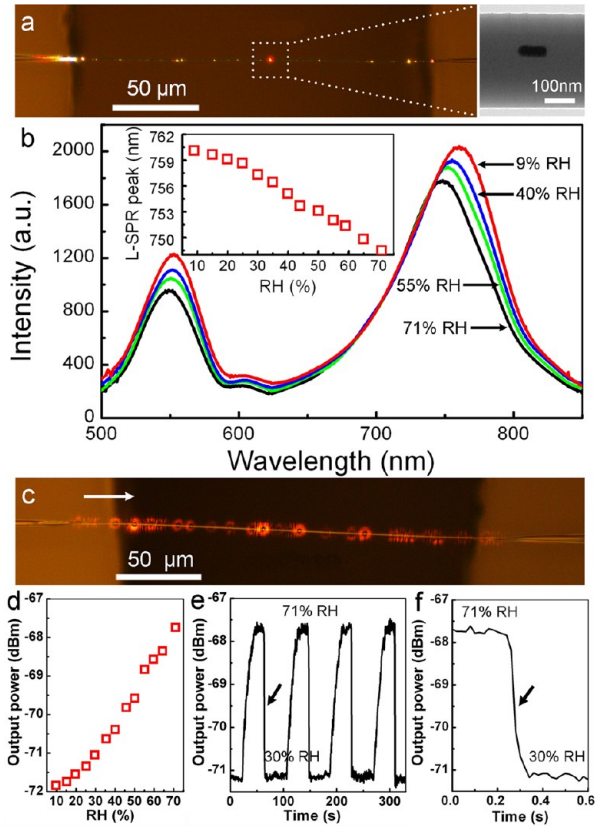

Figure 5. (a) Optical microscopy image of a GNR-embedded nanofiber of 330 nm in diameter waveguided with a 25 nW white light. The inset shows TEM image of the GNR. (b) Scattering spectra of the GNR exposed to air of varying RH. Inset, the dependence of L-SPR peak on the RH of ambient air. (c) Optical microscopy image of the sensing element with a 785 nm wavelength laser waveguided along a GNRs/PAM nanofiber of 540 nm in diameter. White arrow indicates the direction of light propagation. (d) Output power of the nanofiber exposed to air of RH increasing from 9 to 71%. (e) Reversible response of the nanofiber tested by cycling between 30 and 71% RH air. (f) Time-dependent output power of the sensor (enlarged view of the arrowed cycle in (e)) reveals a response time of 110 ms when the RH dropped from 71 to 30%.

dx.doi.org/10.1021/nl301055f | Nano Lett. 2012, 12, 3145−3150

across a microchannel. The whole system was sealed in a glass chamber, and the nanofiber was evanescently coupled to fiber tapers at both ends for launching and collecting the light (see Figure S11 in Supporting Information for details). When the RH was increased from 9 to 71%, the LSPR peaks shifted monotonically from 554.2 to 551.9 nm (for the T-SPR peak) and 760.1 to 748.5 nm (for the L-SPR peak) respectively, as shown in Figure 5b. The spectral shifts can be attributed to a decrease in refractive index for the PAM host: with increasing RH, more water molecules diffused into the PAM nanofiber, which reduced the refractive index of the environment surrounding the embedded GNR, shifting the plasmonic resonance to shorter wavelength and vice versa.[31] From the inset of Figure 5b, the humidity sensitivity of the single GNR was estimated to be ~0.19 nm/% RH (for the L-SPR peak), which is 1 order of magnitude higher than that of bare gold nanoparticles.[39]

From Figure 5b, we also noticed that the scattering intensity of the GNR decreased monotonically with increasing RH, indicating the possibility of realizing intensity-dependent RH sensing. To explore this, we used a PAM nanofiber of 540 nm in diameter containing multiple GNRs to waveguide a monochromatic light of 785 nm in wavelength and measured the intensity of light output from the other end of the nanofiber. As shown in Figure 5c, the LSPR response of individual GNRs (appeared as obvious scattering spots when light was guided through) could be accumulated in the output of the nanofiber and consequently enhance the sensitivity of the sensor. Figure 5d shows the RH-dependent output of the nanofiber with RH increasing from 9 to 71%, offering a sensitivity of ~0.07 dB/% RH and an estimated resolution better than 1% RH. The reversible response of the sensor was tested by cycling between 30 and 71% RH air inside the chamber, and the data in Figure 5e confirmed an excellent reversibility. By suddenly changing the ambient humidity from 71 to 30% RH, we estimated a response time to be about 110 ms for the sensor (Figure 5f), which is much faster than those of existing LSPR-based gas sensors in the form of monolayer or thin film.[40,41] This improvement can be attributed to the small diameter and large surface-to-volume ratio for the nanofiber that enable rapid diffusion or evaporation of the water molecules.

Because of the highly efficient photon-to-plasmon conversion of GNRs in nanofibers, the optical power of the probing light used for sensing could be reduced to a level as low as 25 nW (white light) or 500 pW (785 nm light), which makes it possible to operate the sensor with ultralow optical power. Additionally, benefited from the flexibility in host polymer selection, the sensing scheme demonstrated here can also be applied to other gases.[17,40] Moreover, compared with other functional dopants (e.g., dyes[32] and quantum dots[42]) that may be photobleached after high-dose light exposure, the GNRs are intrinsically immune to photobleaching, making it a long-term high-stability dopants in nanofibers for optical sensing.

In conclusion, with a waveguiding excitation approach we have investigated GNR-embedded polymer nanofibers and evaluated their potential use in optical sensing. The high efficiency of photon-to-plasmon conversion in these waveguiding nanofibers with dopants down to a single GNR, together with the miniaturized optical launching system, opens up new opportunities for developing compact photonic and plasmonic devices with ultralow optical powers. Also, the fiber-taper-assisted in- and out-coupling scheme makes it possible to connect GNR-based devices with standard optical fiber systems with great versatility.

■ ASSOCIATED CONTENT

Supporting Information

Materials; synthesis of GNRs; coating of GNRs with a polyelectrolyte; preparation of GNRs/PAM solutions; fabrication of nanofibers; TEM and SEM characterization; and comparison of the excitation efficiency between waveguiding and illumination schemes. This material is available free of charge via the Internet at http://pubs.acs.org.

■ AUTHOR INFORMATION

Corresponding Author

*E-mail: phytong@zju.edu.cn.

Notes

The authors declare no competing financial interest.

■ ACKNOWLEDGMENTS

The authors thank Huakang Yu, Yaoguang Ma, Kai Fan, and Wei Fang for helpful discussions. This work was supported by the National Natural Science Foundation of China (Grant Nos. 61036012, 60907036, and 10974178), and Fundamental Research Funds for the Central Universities.

■ REFERENCES

(1) Sepulveda, B.; Angelome, P. C.; Lechuga, L. M.; Liz-Marzan, L. M. *Nano Today* **2009**, *4*, 244−251.
(2) Mayer, K. M.; Hafner, J. H. *Chem. Rev.* **2011**, *111*, 3828−3857.
(3) Liu, N.; Tang, M. L.; Hentschel, M.; Giessen, H.; Alivisatos, A. P. *Nat. Mater.* **2011**, *10*, 631−636.
(4) Talley, C. E.; Jackson, J. B.; Oubre, C.; Grady, N. K.; Hollars, C. W.; Lane, S. M.; Huser, T. R.; Nordlander, P.; Halas, N. J. *Nano Lett.* **2005**, *5*, 1569−1574.
(5) McLellan, J. M.; Li, Z. Y.; Siekkinen, A. R.; Xia, Y. N. *Nano Lett.* **2007**, *7*, 1013−1017.
(6) Li, J. F.; Huang, Y. F.; Ding, Y.; Yang, Z. L.; Li, S. B.; Zhou, X. S.; Fan, F. R.; Zhang, W.; Zhou, Z. Y.; Wu, D. Y.; Ren, B.; Wang, Z. L.; Tian, Z. Q. *Nature* **2010**, *464*, 392−395.
(7) Huang, X. H.; EI-Sayed, I. H.; Qian, W.; EI-Sayed, M. A. *J. Am. Chem. Soc.* **2006**, *128*, 2115−2120.
(8) Murphy, C. J.; Gole, A. M.; Stone, J. W.; Sisco, P. N.; Alkilany, A. M.; Goldsmith, E. C.; Baxter, S. C. *Acc. Chem. Res.* **2008**, *41*, 1721−1730.
(9) Lal, S.; Clare, S. E.; Halas, N. J. *Acc. Chem. Res.* **2008**, *41*, 1842−1851.
(10) Cobley, C. M.; Chen, J. Y.; Cho, E. C.; Wang, L. V.; Xia, Y. N. *Chem. Soc. Rev.* **2011**, *40*, 44−56.
(11) Noginov, M. A.; Zhu, G.; Belgrave, A. M.; Bakker, R.; Shalaev, V. M.; Narimanov, E. E.; Stout, S.; Herz, E.; Suteewong, T.; Wiesner, U. *Nature* **2009**, *460*, 1110−1112.
(12) Knight, M. W.; Sobhani, H.; Nordlander, P.; Halas, N. J. *Science* **2011**, *332*, 702−704.
(13) Khatua, S.; Chang, W. −S.; Swanglap, P.; Olson, J.; Link, S. *Nano Lett.* **2011**, *11*, 3797−3802.
(14) Perez-Juste, J.; Rodriguez-Gonzalez, B.; Mulvaney, P.; Liz-Marzan, L. M. *Adv. Funct. Mater.* **2005**, *15*, 1065−1071.
(15) Murphy, C. J.; Orendorff, C. J. *Adv. Mater.* **2005**, *17*, 2173−2177.
(16) Li, J. F.; Liu, S. Y.; Liu, Y.; Zhou, F.; Li, Z. Y. *Appl. Phys. Lett.* **2010**, *96*, 263103.
(17) Kreno, L. E.; Hupp, J. T.; Van Duyne, R. P. *Anal. Chem.* **2010**, *82*, 8042−8046.
(18) Ming, T.; Zhao, L.; Xiao, M. D.; Wang, J. F. *Small* **2010**, *6*, 2514−2519.

(19) Sugikawa, K.; Furukawa, Y.; Sada, K. *Chem. Mater.* **2011**, *23*, 3132−3134.
(20) Kim, G. M.; Wutzler, A.; Radusch, H. J.; Michler, G. H.; Simon, P.; Sperling, R. A.; Parak, W. *Chem. Mater.* **2005**, *17*, 4949−4957.
(21) Tsung, C. K.; Hong, W. B.; Shi, Q. H.; Kou, X. S.; Yeung, M. H.; Wang, J. F.; Stucky, G. D. *Adv. Funct. Mater.* **2006**, *16*, 2225−2230.
(22) Hu, M. S.; Chen, H. L.; Shen, C. H.; Hong, L. S.; Huang, B. R.; Chen, K. H.; Chen, L. C. *Nat. Mater.* **2006**, *5*, 102−106.
(23) He, D.; Hu, B.; Yao, Q. F.; Wang, K.; Yu, S. H. *ACS Nano* **2009**, *3*, 3993−4002.
(24) Roskov, K. E.; Kozek, K. A.; Wu, W. C.; Chhetri, R. K.; Oldenburg, A. L.; Spontak, R. J.; Tracy, J. B. *Langmuir* **2011**, *27*, 13965−13969.
(25) Xia, Y. N.; Yang, P. D.; Sun, Y. G.; Wu, Y. Y.; Mayers, B.; Gates, B.; Yin, Y. D.; Kim, F.; Yan, H. Q. *Adv. Mater.* **2003**, *15*, 353−389.
(26) Lieber, C. M.; Wang, Z. L. *MRS Bull.* **2007**, *32*, 99−108.
(27) Li, D.; Xia, Y. N. *Adv. Mater.* **2004**, *16*, 1151−1170.
(28) Ni, W. H.; Kou, X. S.; Yang, Z.; Wang, J. F. *ACS Nano* **2008**, *2*, 677−686.
(29) Gole, A.; Murphy, C. J. *Chem. Mater.* **2005**, *17*, 1325−1330.
(30) Harfenist, S. A.; Cambron, S. D.; Nelson, E. W.; Berry, S. M.; Isham, A. W.; Crain, M. M.; Walsh, K. M.; Keynton, R. S.; Cohn, R. W. *Nano Lett.* **2004**, *4*, 1931−1937.
(31) Gu, F. X.; Zhang, L.; Yin, X. F.; Tong, L. M. *Nano Lett.* **2008**, *8*, 2757−2761.
(32) Gu, F. X.; Yu, H. K.; Wang, P.; Yang, Z. Y.; Tong, L. M. *ACS Nano* **2010**, *4*, 5332−5338.
(33) Zhang, C. L.; Lv, K. P.; Cong, H. P.; Yu, S. H. *Small* **2012**, *8*, 648−653.
(34) Chen, H. J.; Shao, L.; Woo, K. C.; Ming, T.; Lin, H. Q.; Wang, J. F. *J. Phys. Chem. C* **2009**, *113*, 17691−17697.
(35) Tong, L. M.; Gattass, R. R.; Ashcom, J. B.; He, S. L.; Lou, J. Y.; Shen, M. Y.; Maxwell, I.; Mazur, E. *Nature* **2003**, *426*, 816−819.
(36) Kien, F. L.; Liang, J. Q.; Hakuta, K.; Balykin, V. I. *Opt. Commun.* **2004**, *242*, 445−455.
(37) Tong, L. M.; Lou, J. Y.; Mazur, E. *Opt. Express* **2004**, *12*, 1025−1035.
(38) Mühlschlegel, P.; Eisler, H. −J.; Martin, O. J. F.; Hecht, B.; Pohl, D. W. *Science* **2005**, *308*, 1607−1609.
(39) Bingham, J. M.; Anker, J. N.; Kreno, L. E.; Van Duyne, R. P. *J. Am. Chem. Soc.* **2010**, *132*, 17358−17359.
(40) Karakouz, T.; Vaskevich, A.; Rubinstein, I. *J. Phys. Chem. B* **2008**, *112*, 14530−14538.
(41) Cheng, C. S.; Chen, Y. Q.; Lu, C. J. *Talanta* **2007**, *73*, 358−365.
(42) Meng, C.; Xiao, Y.; Wang, P.; Zhang, L.; Liu, Y. X.; Tong, L. M. *Adv. Mater.* **2011**, *23*, 3770−3774.